JAMES | Journal of Advances in Modeling Earth Systems

RESEARCH ARTICLE
10.1029/2023MS003765

Convection and Convective-Organization in Hothouse Climates

Guy Dagan[1], Jacob T. Seeley[2], and Nathan Steiger[1]

[1]Fredy and Nadine Herrmann Institute of Earth Sciences, Hebrew University, Jerusalem, Israel, [2]Department of Earth and Planetary Sciences, Harvard University, Cambridge, MA, USA

Key Points:

- We examine the temporal and spatial organization of convection in simulated hothouse conditions
- We demonstrate that lower tropospheric radiative heating is not necessary for the "episodic deluge" precipitation regime
- "Episodic deluge" precipitation regime occurs in self- or forced-convective aggregated large domain simulations but is less synchronized

Supporting Information:

Supporting Information may be found in the online version of this article.

Correspondence to:

G. Dagan,
guy.dagan@mail.huji.ac.il

Citation:

Dagan, G., Seeley, J. T., & Steiger, N. (2023). Convection and convective-organization in hothouse climates. *Journal of Advances in Modeling Earth Systems*, *15*, e2023MS003765. https://doi.org/10.1029/2023MS003765

Received 11 APR 2023
Accepted 24 OCT 2023

Author Contributions:

Conceptualization: Guy Dagan, Jacob T. Seeley, Nathan Steiger
Formal analysis: Guy Dagan
Methodology: Guy Dagan
Visualization: Guy Dagan
Writing – original draft: Guy Dagan
Writing – review & editing: Guy Dagan, Jacob T. Seeley, Nathan Steiger

Abstract In a "hothouse" climate, warm temperatures lead to a high tropospheric water vapor concentration. Sufficiently high water vapor levels lead to the closing of the water vapor infrared window, which prevents radiative cooling of the lower troposphere. Because water vapor also weakly absorbs solar radiation, hothouse climates feature radiative heating of the lower troposphere. In recent work, this radiative heating was shown to trigger a shift into a novel "episodic deluge" precipitation regime, where rainfall occurs in short, intense outbursts separated by multi-day dry spells. Here, we further examine the role of the lower tropospheric radiative heating (LTRH) in the transition into the "episodic deluge" regime. We demonstrate that under high sea-surface temperature the "episodic deluge" regime could be formed even before the LTRH turns positive. In addition, we examine whether these oscillations operate on larger scales and how these oscillations, which represent "temporal" convective self-organization, would manifest in the presence of traditional "spatial" self- or forced-aggregation in large-domain convection-permitting simulations. We find that the temporal oscillations become much less synchronized throughout a large domain ($\mathcal{O}$ 1,000 km) because gravity waves cannot propagate fast enough to synchronize convection. We also show that temporal oscillations still dominate the rainfall distribution even when there is tropical convective self-aggregation or a large-scale overturning circulation. These results could have important implications for extreme precipitation events under a warming climate.

Plain Language Summary Water vapor is a strong greenhouse gas that closely follows surface temperature. Under very warm ("hothouse") conditions, which are believed to have existed in the Earth's distant past, temperature and water vapor are sufficiently high that the greenhouse effect of water vapor prevents heat from escaping out of the lower part of the atmosphere. This trapped heat makes the lower atmosphere even hotter, causing some unusual weather patterns. For example, it was recently shown to lead to short but intense bursts of rain, followed by several days of dry weather. However, it is unclear whether these patterns occur on larger scales and what their characteristic scale is. In this study, computer simulations were conducted to address these uncertainties and to further elucidate the role of the lower tropospheric radiative heating in the transition into this "episodic deluge" regime. We show that these temporal oscillations dominate the rainfall distribution even in the presence of other atmospheric factors such as tropical convective self-aggregation or large-scale overturning circulation.

1. Introduction

Earth's climate history includes extremely warm, ice-free states known as "hothouse" climates (Charnay et al., 2017; Meckler et al., 2022; Sleep, 2010). For example, in the Hadean and Archaean eons it is estimated that the surface temperatures were significantly higher—by tens of degrees kelvin—compared to today (Charnay et al., 2017; Sleep, 2010). According to a recent reconstruction (Meckler et al., 2022), even during the Eocene (about 50 Ma ago) the average surface temperatures were about 20 K higher than today. In addition, in the future, as the Sun's luminosity increases with its stellar evolution on the main sequence, Earth's climate is anticipated to transition into hothouse conditions before reaching a runaway greenhouse state (Seeley & Wordsworth, 2021; Wolf & Toon, 2015). Under such hothouse conditions, the water vapor concentration in the lower troposphere is expected to be sufficiently high that the water vapor infrared window would become opaque (kumar Kopparapu et al., 2016; Popp et al., 2016; Seeley & Wordsworth, 2021; Wolf & Toon, 2015; Wolf et al., 2018). Once the water vapor infrared window is closed, the lower-tropospheric radiative cooling that is observed under current climate conditions is anticipated to shift to radiative warming, driven by a lack of longwave cooling and a weak shortwave absorption by water vapor (Seeley & Wordsworth, 2021; Wolf et al., 2018). Previously it was shown that this lower-tropospheric radiative heating (LTRH) could lead to convective inhibition, thus significantly affecting

the behavior of convection (Seeley & Wordsworth, 2021; Wolf et al., 2018). Recently a convection-resolving modeling study of the hothouse regime indicates that the LTRH drives a shift of the hydrological cycle into a fundamentally different climate state: the "episodic deluge" or "relaxation oscillator" regime where short and intense outbursts of rainfall are separated by multi-day dry spells (Seeley & Wordsworth, 2021, hereafter SW21). Based on these results, SW21 suggested that a novel form of temporal convective self-organization may exist, and maybe even dominate, hothouse climates. SW21 speculated that this behavior may have important implications for geological erosion processes.

The work of SW21 was based on small-domain radiative-convective-equilibrium (RCE) simulations (Wing, Reed, et al., 2018), which are known to suppress more traditional spatial convective self-organization (or self-aggregation) (Muller & Held, 2012; Wing, Reed, et al., 2018). Convective self-aggregation, in its traditional definition, occurs when convection tends to cluster without an external forcing, such as from sea-surface temperature (SST) gradients (Coppin & Bony, 2015; Muller & Held, 2012; Muller et al., 2022; Wing, Emanuel, et al., 2018). Convective self-aggregation commonly appears in RCE simulations of global simulations with parameterized convection as well as in high resolution convection-permitting simulations (i.e., using few km resolution) when the domain size is large enough (Muller & Held, 2012; Muller et al., 2022; Wing et al., 2020; above a few 100s km). Convective self-aggregation is known to have a significant effect on the mean simulated climate conditions. For example, when convection aggregates under current climate conditions there is domain-mean drying, free-tropospheric warming, and more longwave radiation that is emitted to space (Bretherton et al., 2005; Muller & Held, 2012; Wing et al., 2020). In addition, convective self-aggregation was shown to increase the horizontal moisture variability and to be accompanied by the formation of dry patches with enhanced outgoing longwave radiation (OLR) (Wing & Emanuel, 2014). The reduced humidity of the dry patches in an aggregated state should reduce the magnitude of LTRH at a given surface temperature (as compared to a disorganized state), and therefore might delay or prevent the emergence of the relaxation oscillator regime. Importantly to this paper, convective self-aggregation was also shown to have an effect on the mean and extreme precipitation (Bao et al., 2017; Da Silva et al., 2021; Fildier et al., 2021; Pendergrass, 2020; Pendergrass et al., 2016).

While the mechanisms responsible for triggering and maintaining self-aggregation are still not fully understood, it has been shown that interactions between longwave radiation and moisture are essential (Coppin & Bony, 2015; Dingley et al., 2021; Muller & Held, 2012; Yang, 2018). This longwave-moisture mechanism is driven by a strong clear-sky longwave radiative cooling in the dry parts of the domain, which, due to a weak-temperature gradient approximation (Sobel et al., 2001), produces subsidence in these dry regions and acts to develop an overturning circulation. Due to the central role of the above feedback, it was shown that prescribing the radiative cooling rates (rather than letting them evolve as a function of the local water vapor concentration) can prevent convective self-aggregation (Dingley et al., 2021; Muller & Held, 2012).

In addition to spontaneously self-aggregating, convection can also be "forced" to aggregate by an SST gradient (Hohenegger & Jakob, 2020; Lutsko & Cronin, 2023; Müller & Hohenegger, 2020). In idealized "mock Walker" simulations, a simple SST gradient is imposed, forcing a large-scale overturning circulation (Bretherton et al., 2006; Grabowski et al., 2000; Lutsko & Cronin, 2023). Convection is then highly coupled to this large-scale overturning circulation (Bony et al., 2015), producing most of the precipitation in the ascending branch.

A central unanswered question from SW21 regards the natural physical scale of the synchronized convective regime. In other words, would a simulation conducted in a larger domain produce similar oscillatory behavior as reported in SW21? In this paper we aim at answering this question and at examining the potential effect of convective self- and forced-aggregation on SW21's oscillatory behavior.

2. Materials and Methods

RCE simulations are conducted using the System for Atmospheric Modeling (SAM; M. F. Khairoutdinov & Randall, 2003) version 6.11.7, with its one-moment microphysical parameterization. Subgrid-scale fluxes are parameterized using Smagorinsky's eddy diffusivity model. In addition, gravity waves are damped at the top of the domain and doubly-periodic boundary conditions are assumed. These simulations generally follow the RCE Model Intercomparison Project (RCEMIP) protocol (Wing, Reed, et al., 2018) with some modifications as elaborated below.

Most of the simulations are conducted under spatially homogenized, prescribed SSTs (besides the mock Walker simulations—Table 1). The domain size is varied over a wide range of sizes and geometries in order to examine its

Table 1
List of Simulations

Simulation	SST (K)	Horizontal grid points	Resolution (km)	Interactive radiation
RCE_small	295–325 in 2.5 intervals	96 × 96	1	✓
RCE_small_295_FixedRAD_Real	295	96 × 96	1	
RCE_small_295_FixedRAD_Ideal	295	96 × 96	1	
RCE_small_325_FixedRAD_Ideal	325	96 × 96	1	
RCE_large_320	320	2,048 × 128	3	✓
RCE_large_325	325	2,048 × 128	3	✓
RCE_large_320_FixedRAD	320	2,048 × 128	3	
RCE_large_325_FixedRAD	325	2,048 × 128	3	
RCE_largeX2.25	325	2,048 × 128	4.5	✓
RCE_large/2	325	1,024 × 128	3	✓
RCE_large/2_295	295	1,024 × 128	3	✓
RCE_large/4	325	512 × 128	3	✓
RCE_large/4_295	295	512 × 128	3	✓
RCE_large/8	325	256 × 128	3	✓
RCE_large/18	325	256 × 128	2	✓
RCE_large/32	325	256 × 128	1.5	✓
RCE_large/72	325	256 × 128	1	✓
RCE_square_1	325	256 × 256	3	✓
RCE_square_2	325	128 × 128	3	✓
RCE_square_3	325	96 × 96	2	✓
mock_Walker_295	295	2,048 × 128	3	✓
mock_Walker_1	325	2,048 × 128	3	✓
mock_Walker_2	325	2,048 × 128	1.5	✓
mock_Walker_3	325	512 × 128	3	✓

effect on convective organization and precipitation. In addition, the horizontal resolution is also varied between 1 and 4.5 km (Table 1). In the vertical dimension, the grid is composed of 81 levels, which follows the RCEMIP protocol (Wing, Reed, et al., 2018) up to a height of 33 km and is extended to 40 km with 1 km resolution to account for the deeper troposphere under higher SSTs (Hartmann & Larson, 2002). A preindustrial level of CO_2 (280 ppm) is specified and the vertical profile of O_3 is as in Wing, Reed, et al. (2018). We note that the use of a fixed ozone vertical distribution might affect the tropopause height and limit its growth in warm climates to some degree. Other trace gases such as CH_4 and N_2O are neglected for simplicity.

A time step of up to 5s is used. Radiative fluxes are calculated every 5 min using the CAM (Community Atmosphere Model) radiation scheme (Collins et al., 2006), except for experiments using prescribed radiative cooling rates—FixedRAD, see Table 1. The output resolution is 1 hr. Following Wing, Reed, et al. (2018), a net insolation close to the current climate tropical-mean value is set by fixing the incoming solar radiation at 551.58 W m^{-2}, with a zenith angle of 42.05°. Small temperature perturbations ($\mathcal{O}$ 0.02 K) are added near the surface at the beginning of the simulation to initialize convection. The initial conditions for the simulations are based on the last 30 days of a 150-day long small domain simulation (RCE_small, see Table 1) for each SST value (Wing, Reed, et al., 2018). The rest of the simulations are run for 100 days (as in Wing, Reed, et al. (2018)) and the last 50 days of each simulation are used for the statistical analyses.

For examining the role of forced-aggregation compared with self-aggregation, in addition to the simulations conducted under homogenized SST conditions, four additional "mock Walker" simulations (Bretherton et al., 2006; Grabowski et al., 2000; Lutsko & Cronin, 2023) are conducted with an SST gradient along the long dimension (X) of the domain and with a domain mean SST value of either 295 K or 325 K. The SST distribution

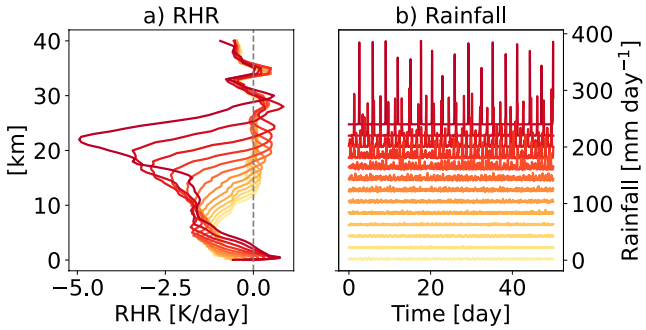

Figure 1. Results from radiative-convective-equilibrium small domain (RCE_small) simulations with interactive radiation conducted under different sea-surface temperature (SST) between 295 and 325 K in 2.5 K intervals (going from lighter to darker colors). (a) The domain- and time-mean (over the last 50-day of the simulations) radiative heating rate (RHR) vertical profiles, and (b) the domain-mean rainfall time series. For clarity, in panel (b) an increasing with SST offset of 20 mm day^{-1} has been added to each curve.

is set as a sinusoidal function of X as presented in Figures 17d–17f. The SST range in this case is 5 K, which resembles the range observed over the tropical Pacific Ocean (Lutsko & Cronin, 2023).

3. Results

3.1. The Ability of SAM to Simulate the Transition Into LTRH and the "Episodic Deluge" Regime

First we examine the ability of the model SAM to simulate the transition into LTRH and the "episodic deluge" regime under an increased SST using the RCE_small simulations. SW21 performed significant modifications to their model, and specifically to the radiative scheme, for it to represent well hothouse conditions. Thus, it is important to make sure that SAM and the CAM radiative scheme perform well under such high SSTs and are able to capture the trends reported in SW21. Hence, in Figure 1 we present the domain- and time-mean radiative heating rate (RHR) vertical profiles and the domain mean rainfall time series for RCE_small simulations conducted with interactive radiation and under different SSTs between 295 and 325 K in 2.5 K intervals. It demonstrates that in SAM, as the SST increases the lower tropospheric RHR becomes increasingly larger and turn positive for SSTs above 315 K. Consistent with SW21, the rainfall time series demonstrate that as the lower tropospheric RHR increases and shifts into LTRH, the rainfall shifts into an "episodic deluge" regime from the quasi-steady regime found under lower SSTs. These results give us confidence in the ability of SAM in simulating hothouse conditions.

3.2. On the Role of LTRH in the Transition Into "Episodic Deluge" Regime

SW21 demonstrated that in their model LTRH was a sufficient condition for the transition into episodic deluges. That is to say that an LTRH under low SST (in which episodic deluges are not being generated naturally) generated episodic deluges. However, their simulations were conducted with a highly idealized RHR vertical profile. Here we would like to examine whether more realistic RHR vertical profiles, as presented in Figure 1a, can shift a low SST run into the episodic deluge regime. A related question that was left open from SW21 is whether or not the LTRH is a necessary condition for the transition into episodic deluges. In other words, can a warm SST case without LTRH generate episodic deluges?

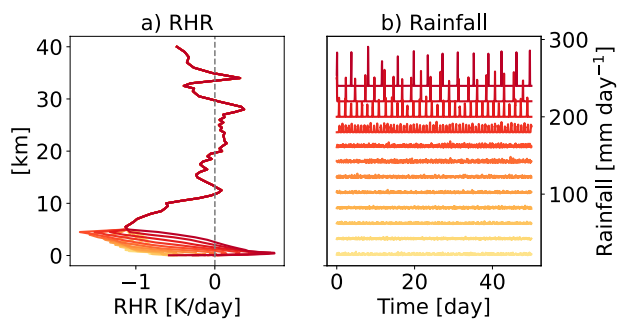

Figure 2. Results from radiative-convective-equilibrium small domain simulations (RCE_small) with prescribed radiation conducted under sea-surface temperature of 295 K but different radiative heating rate (RHR) vertical profiles based on the realistic lower tropospheric RHR profiles presented in Figure 1a (going from lighter to darker colors—RCE_small_295_FixedRAD_Real). (a) The imposed RHR vertical profile in each simulation, and (b) the domain-mean rainfall time series in each simulation. For clarity, in panel (b) an increasing offset of 20 mm day^{-1} has been added to each curve.

In order to answer the first question, regarding the "sufficiency" of a LTRH to generate episodic deluges regime under low SST, we use two sets of RCE_small simulations (RCE_small_295_FixedRAD_Real and RCE_small_295_FixedRAD_Ideal). For examining the role of the LTRH in RCE_small simulations presented in Figure 1 we have conducted an additional set of simulations in which we fix the SST at 295 K and changed the RHR vertical profile, based on the realistic profiles presented in Figure 1a, only in the lower 5 km to account only for the LTRH and not for the changes in the RHR in the upper troposphere, which is kept as in the 295 K case presented above (Figure 2 RCE_small_295_FixedRAD_Real). These simulations demonstrate, in agreement with SW21, that LTRH is a sufficient condition to trigger a shift into the episodic deluge regime, that is, even under low SST, LTRH drives a transition into the episodic deluge regime as defined by SW21. These results appear here using a more realistic vertical profiles of RHR than the ones used in SW21 and could have important implications for the case of changes in the RHR vertical profiles in our current climate, for example, due to shortwave absorption by aerosols.

In the simulations presented in Figure 2 the vertical integral of the RHR is different between the different simulations, which is known to affect precipitation (Jeevanjee & Romps, 2018). Hence, in order to make sure that this

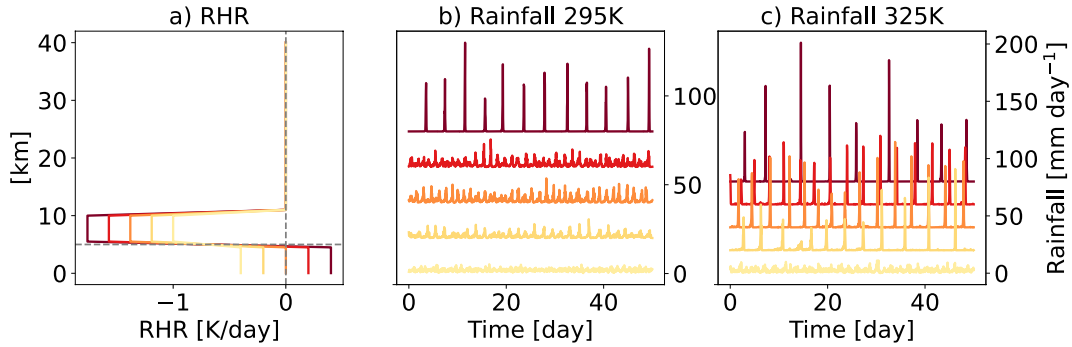

Figure 3. Results from radiative-convective-equilibrium small domain simulations (RCE_small) conducted under sea-surface temperature of 295 K or of 325 K but under different prescribed idealized radiative heating rate (RHR) vertical profiles. (a) The imposed RHR vertical profile in each simulation, (b) the domain-mean rainfall time series in each simulation conducted under SST of 295 K (RCE_small_295_FixedRAD_Ideal), and (c) the domain-mean rainfall time series in each simulation conducted under SST of 325 K (RCE_small_325_FixedRAD_Ideal). For clarity, in panels (b and c) an increasing offset of 20 mm day^{-1} has been added to each curve.

is not responsible somehow for the transition into the episodic deluge regime, we turn back to idealized RHR profiles as in SW21, and make an additional set of simulations under SST of 295 K in which we prescribe an idealized RHR in a way that its vertical integral is roughly fixed (Figure 3a; RCE_small_295_FixedRAD_Ideal). This demonstrates again that in SAM we get similar results as in SW21 and show that a LTRH is a sufficient condition in order to shift into the episodic deluge regime even under relatively low SST and a fixed RHR vertical integral (Figure 3b).

For answering the second question mentioned above (whether or not the LTRH is necessary for the transition into episodic deluges?), we have repeated the idealized fixed RHR simulations under high SST of 325 K (RCE_small_325_FixedRAD_Ideal—Figure 3c). It demonstrates that under the most negative lower tropospheric RHR profile used here no episodic deluges are formed even under SST of 325 K. However, as we increase the lower tropospheric RHR and increase the difference in RHR between the lower 5 km and the 5 km above it, the precipitation regime shifts into episodic deluges even before the lower tropospheric RHR become positive. These results suggest that a relatively high (less negative) lower tropospheric RHR, and a relatively high difference in the RHR between the lower and mid/upper troposphere, are necessary for the transition into episodic deluges. However, a full transition into positive values at the lower troposphere are not necessary. We note, that in parallel to our work, two other papers showed similar results using different setups (Song et al., 2023; Spaulding-Astudillo & Mitchell, 2023).

3.3. Sensitivity to SST and Domain Size

Following the RCEMIP protocol and the work by SW21, we start by comparing the domain-mean rainfall and near surface moist static energy (MSE) time series in RCE_small and RCE_large simulations under reference (295 K) and hothouse (325 K) SSTs (RCE_small_295, RCE_small_325, RCE_large_295, and RCE_large_325—Figure 4). This figure demonstrates that the RCE_small simulations produce the transition between the quasi-steady regime under low SST to the oscillatory behavior reported in SW21 under high SST. Specifically, we note the similar phase relationships between the MSE and precipitation as reported in SW21. In the RCE_large simulations (lower row in Figure 4), the lower SST simulation demonstrates a behavior similar to the quasi-steady regime of the small domain simulation, while under hothouse conditions we see a behavior that can be described as a much less coherent relaxation oscillator regime. That is to say that in an RCE_large hothouse simulation we can identify periods with almost no precipitation throughout the entire domain. In these periods the near surface MSE is accumulating, reaching to high values until a strong precipitation event starts lasting for a few hours and up to few days.

A direct comparison of the domain-mean precipitation in the RCE_small and RCE_large simulations under the three different SSTs (a reference SST of 295 K and two hothouse SSTs of 320 and 325 K) is presented in Figure 5. It demonstrates the different behavior between the small and large domain simulations conducted under high SST,

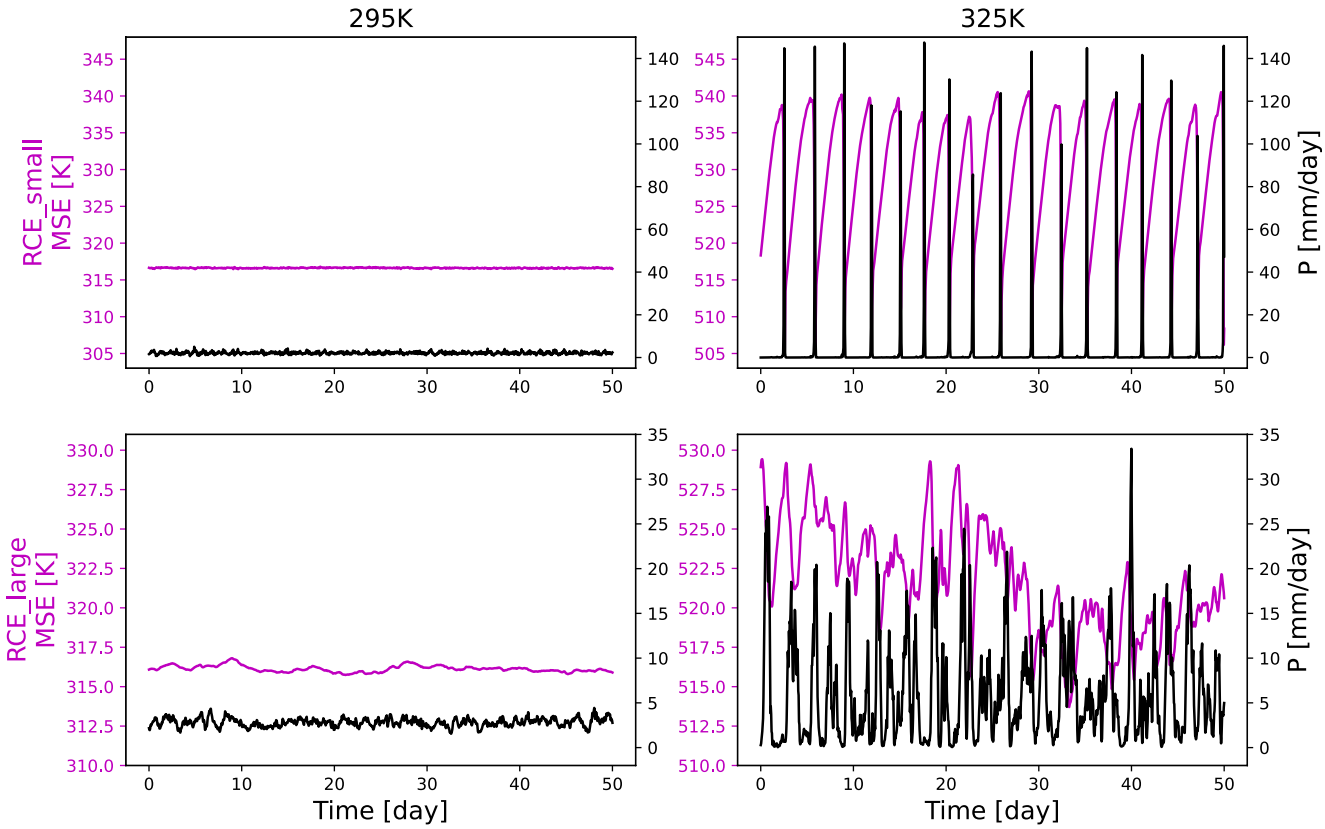

Figure 4. Domain-mean near surface moist static energy (MSE) and rainfall (P) time series in radiative-convective-equilibrium small domain (RCE_small; upper row) and large domain (RCE_large; lower row) simulations conducted under sea-surface temperature of 295 (left column) and 325 K (right column).

which is absent in the reference SST case (295 K). It also demonstrates that the simulations conducted under SST of 320 K already demonstrates the transition into the episodic deluges regime but to a lesser magnitude than the simulations conducted under SST of 325 K.

Figure 6 presents power spectrum of local precipitation (calculated as the average power spectrum over all grid points in the domain over the last 50 days of the simulation) for RCE_large and RCE_small under the reference and high SST cases (the power spectrum of the domain-mean precipitation is presented in Figure S7 in Supporting Information S1). This figure demonstrates that in the RCE_small simulations there is a clear regularity with a returning frequency of about 3 days under the high SST case, and no clear regularity under the low SST case. The power spectrum of the RCE_large also demonstrates a weak local maximum at 3 days period under high SST and lack of this peak under low SST (the low SST large domain simulation demonstrates a weak peak at about 7-days period, which correspond to the propagation time of gravity waves throughout the domain as elaborated below). The weaker relative local maximum at 3 days period in the RCE_large high SST simulation compared with the RCE_small simulation suggests a reduction in the level of synchronization of the convection and less coherence. In addition, consistent with the transition into episodic deluges regime under high SST, the probability density function of the local rainfall demonstrates a reduction in the probability of weak rainfall rates and a strong increase in the probability of strong rainfall rates compared with the reference simulation in both RCE_small and RCE_large (Figure S1 in Supporting Information S1).

3.4. Effects of Convective Self-Aggregation

The RCEMIP protocol, which the simulations here follow, was designed in part to understand the effect of convective self-aggregation on the domain-mean properties (Wing, Reed, et al., 2018; Wing et al., 2020). This can be done by comparing the RCE_large and RCE_small simulations, and attributing the difference between them to the effect of convective self-aggregation alone (Wing et al., 2020). In our case, however, for attributing

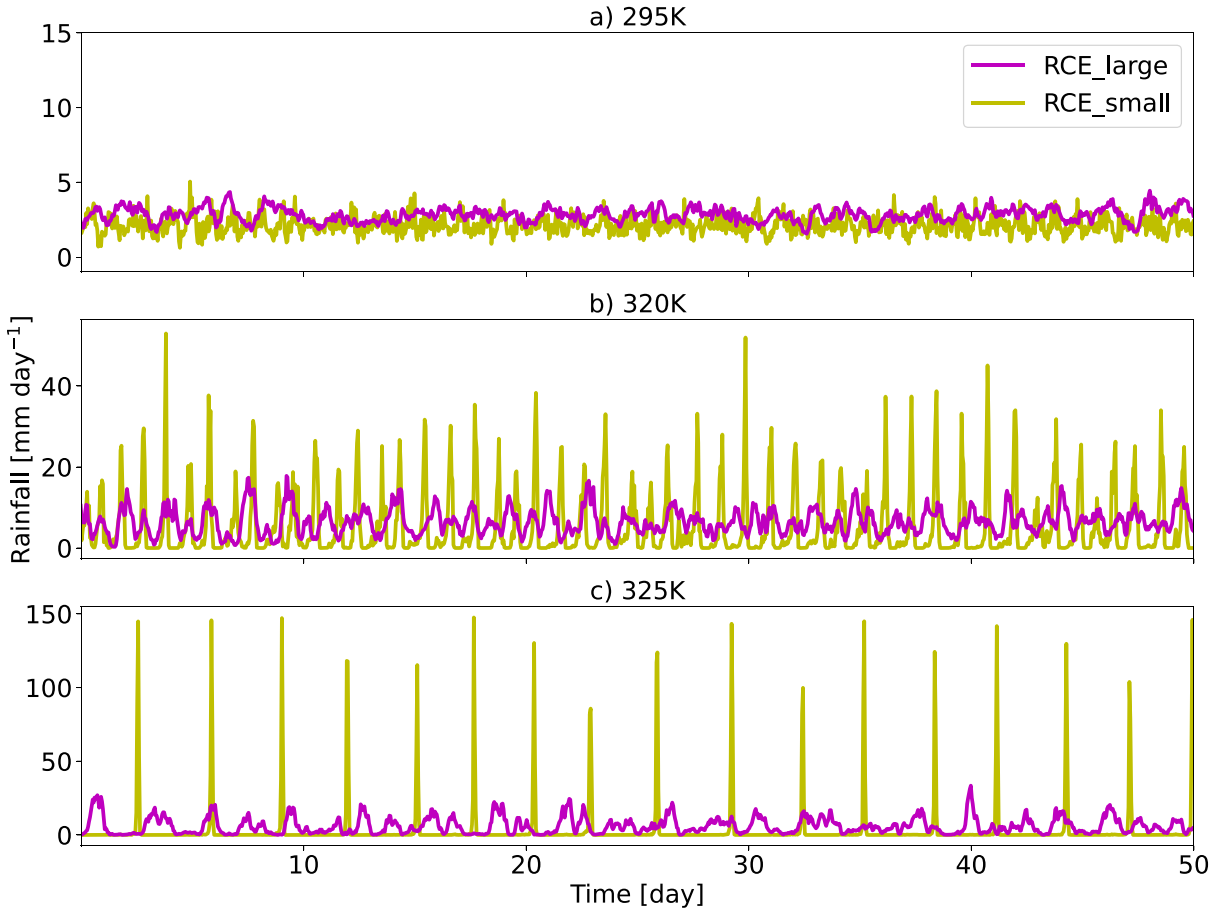

Figure 5. Domain-mean rainfall time series in radiative-convective-equilibrium small domain (RCE_small) and large domain (RCE_large) simulations under sea-surface temperature of 295 K (a), 320 K (b), and 325 K (c).

the difference between RCE_large and RCE_small to self-aggregation, we need to make sure that the RCE_large simulations are indeed aggregated in the traditional sense (as opposed to its temporal form as suggested by SW21). In addition, in our case the difference between RCE_large and RCE_small could also be driven by other factors beside self-aggregation. In particular, the difference in the domain-mean rainfall between RCE_large and RCE_small could also be driven by a difference in the level of synchronization of the simulations (caused solely by the different domain sizes even in the absence of self-aggregation).

To check if the RCE_large hothouse simulations are aggregated, we examine Hovmoller diagrams of the OLR and precipitable water of these simulations in Figure 7. This figure shows that the RCE_large simulations do indeed

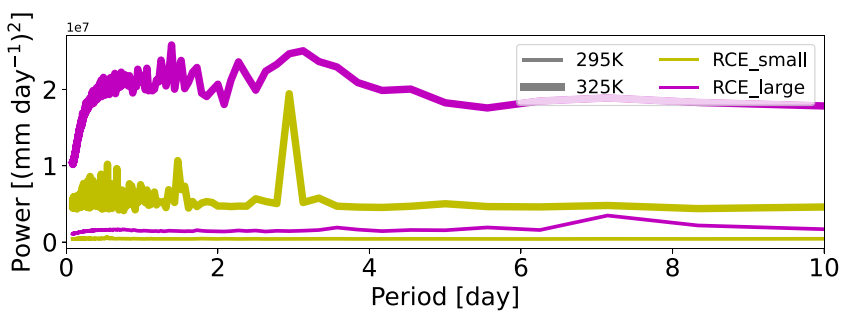

Figure 6. Power spectrum of the local rainfall, calculated as the average power spectrum over all grid points in the domain over the last 50 days of the simulation in radiative-convective-equilibrium small domain (RCE_small) and large domain (RCE_large) simulations under sea-surface temperature of 295 and 325 K.

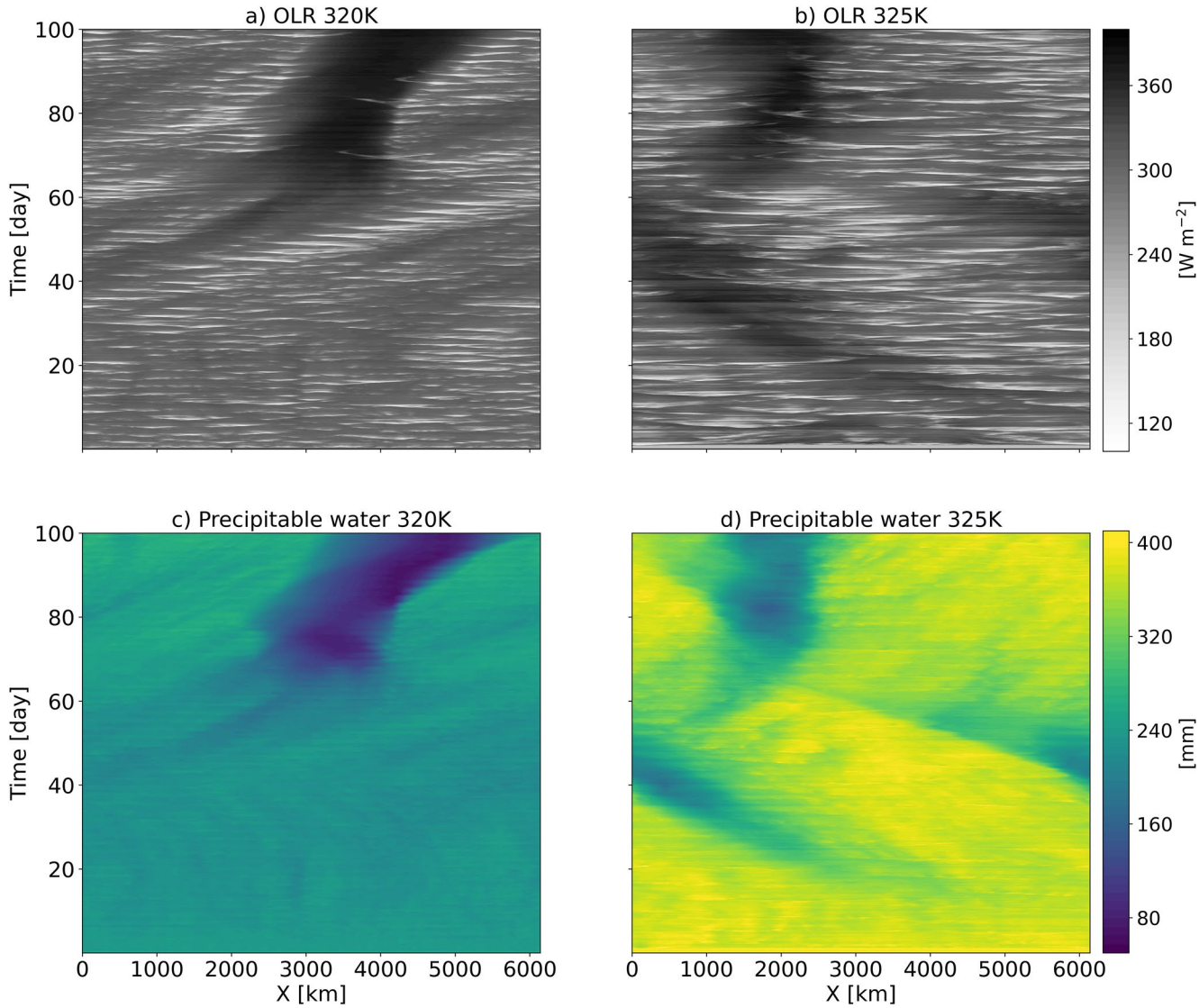

Figure 7. (a and b) Hovmoller diagrams of the top of atmosphere outgoing longwave radiaition (OLR). (c and d) Hovmoller diagrams of the precipitable water for the two radiative-convective-equilibrium large domain (RCE_large) simulations conducted under different SSTs, 320 K in panels (a and c), and 325 K in panels (b and d). These Hovmoller diagrams are averaged over the *Y* direction and are based on 2D instantaneous output.

feature dry patches with enhanced OLR, as produced by convective self-aggregation. As expected (Bretherton et al., 2005; Muller & Held, 2012; Wing et al., 2020), the formation of these dry patches with enhanced local OLR also produced an increased domain mean and maximum OLR compared with the unaggregated RCE_small simulations (Figures S2 and S3 in Supporting Information S1). In addition, we calculate a common metric for convective-aggregation, I_{org} (Tompkins & Semie, 2017; Figure S4 in Supporting Information S1), which also suggests that the large domain simulations are aggregated in the traditional sense (values well above 0.5). However, it is not immediately clear what I_{org} represents in the presence of SW21's temporally oscillatory behavior. Nevertheless, from Figure 7 and Figures S2 and S3 in Supporting Information S1 we can conclude that the RCE_large hothouse simulations are aggregated in the sense that they include large dry patches and hence an enhanced OLR compared with the RCE_small simulations.

As was hypothesized in the introduction, the enhanced OLR in the presence of convective self-aggregation in the RCE_large simulations could reduce the LTRH in these simulations compared with RCE_small simulations. This is confirmed by comparing the domain- and time-mean RHR vertical profiles of the different simulations, Figure 8. This figure shows that indeed convective self-aggregation acts to weaken the LTRH, that is,

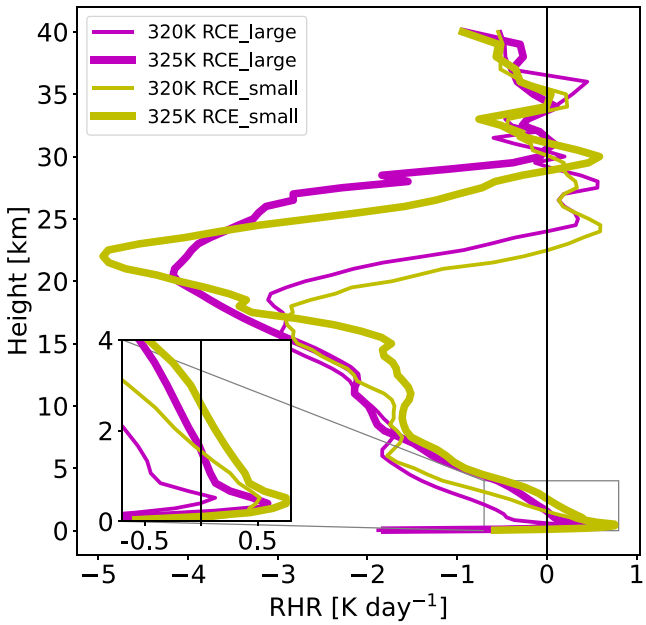

Figure 8. The domain- and time-mean (over the last 50-day of the simulations) radiative heating rate (RHR) vertical profiles of the radiative-convective-equilibrium small domain (RCE_small) and large domain (RCE_large) simulations conducted under different sea-surface temperatures.

the maximum LTRH is lower and the layer in which the RHR is positive is shallower in RCE_large than in RCE_small.

To examine the role of the reduced LTRH in the RCE_large compared with the RCE_small simulations, and to separate it from the effect of the domain size alone, we re-ran the RCE_large simulations with a prescribed RHR vertical profile taken from the RCE_small simulations for each SST of 320 and 325 K (RCE_large_320_FixedRAD and RCE_large_325_FixedRAD). Prescribing the RHR vertical profile suppresses the formation of dry patches (see Figure S5 in Supporting Information S1), but these simulations still do not reproduce the strong oscillatory behavior seen in RCE_small. Specifically, in Figure 9 we compare the rainfall time series in RCE_large_FixedRAD with the RCE_small and RCE_large simulations. This figure demonstrates that domain-mean precipitation in RCE_large_FixedRAD is more similar to RCE_large than RCE_small.

Based on Figure 9, we can conclude that the main difference between RCE_small and RCE_large is not due to the difference in convective self-aggregation and RHR vertical profile but rather related to the size of the domain, which affects the synchronization of the convection (as elaborated below).

To gain a better understanding of the distribution of rainfall in the RCE_large and RCE_large_FixedRAD simulations, we present Hovmoller diagrams of the rainfall in these simulations conducted under SST = 325 K in Figures 10a and 10b. It reveals that, on a local scale that cover only a portion of the large domain simulation, the rainfall exhibits short and intense outbursts. We note that averaging the rainfall over the entire domain (Figure 9) partially masks strong oscillatory behavior that occurs on a more local scale.

Figures 10c–10f provide a zoomed-in view of a representative rainfall outburst from each simulation (marked in red in Figures 10a and 10b). The figure shows that the outburst begins at a specific location where large amounts of precipitable water accumulate. Once the rainfall starts, it spreads horizontally at a speed of around 60 km hr^{-1}, which corresponds to the propagation speed of gravity waves. Typically, an outburst event lasts for approximately 12 hr and up to a

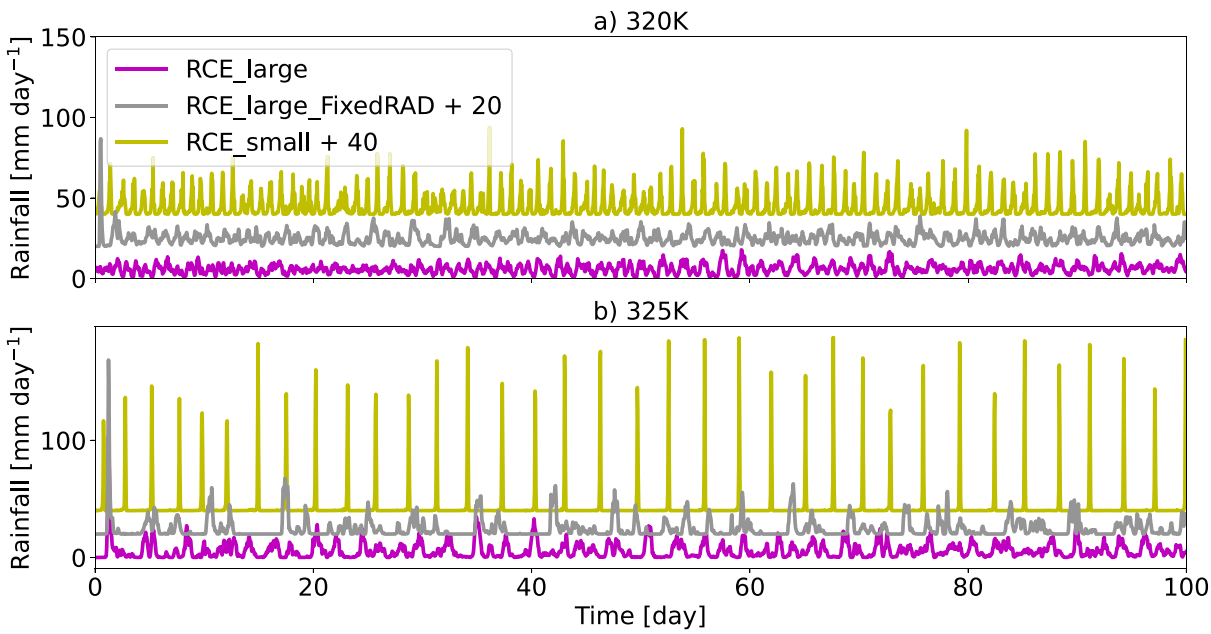

Figure 9. Domain-mean rainfall time series in radiative-convective-equilibrium small doamin (RCE_small), large domain (RCE_large) and large domain with prescribed radiatin (RCE_large_FixedRAD) simulations under sea-surface temperature of 320 K (a) and 325 K (b). For clarity a specific offset value has been added to each curve, as noted in the legend.

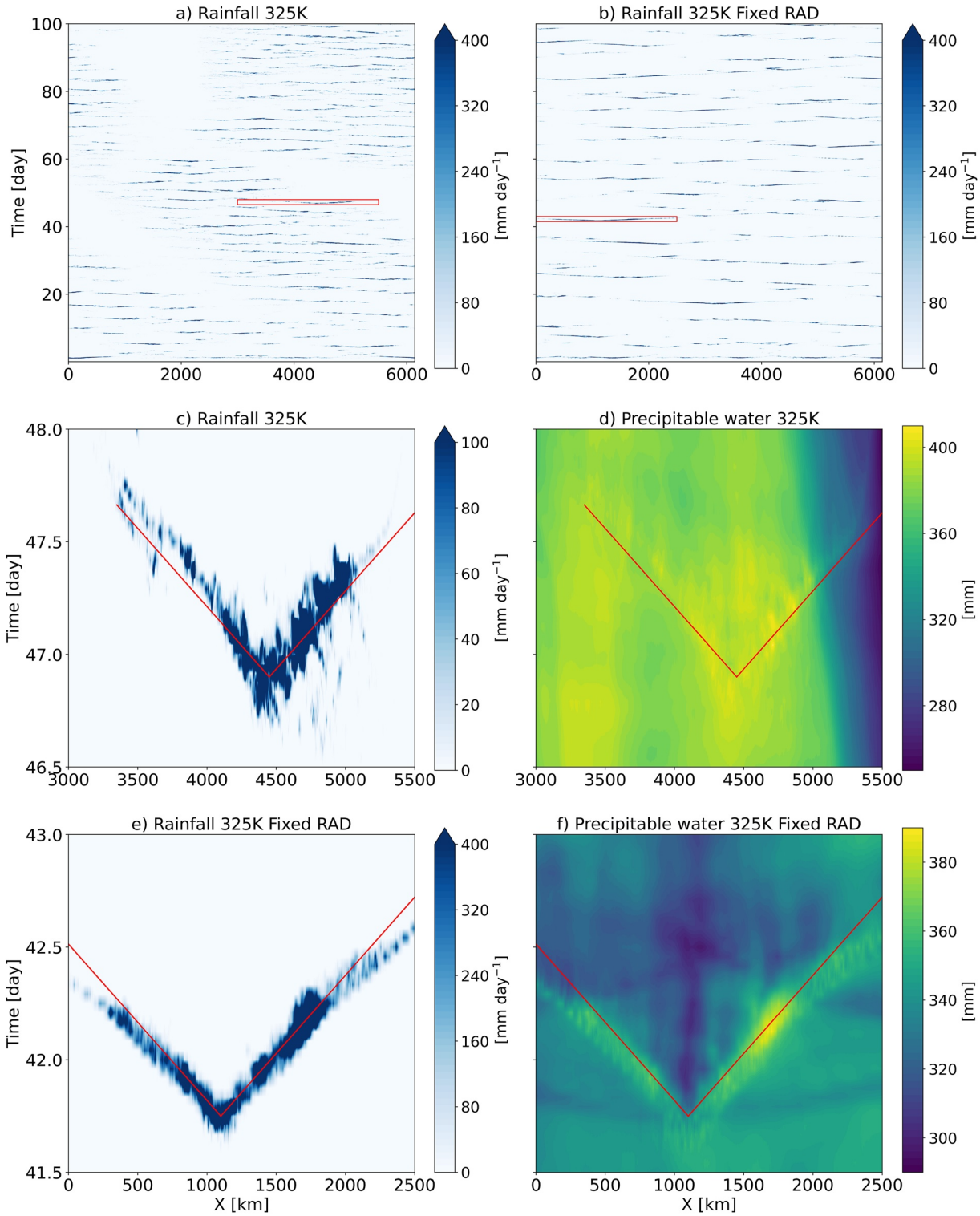

Figure 10. Hovmoller diagrams of the rainfall for radiative-convective-equilibrium large domain (RCE_large) (a), and large domain with prescribed radiation (RCE_large_FixedRAD) (b) simulations conducted under sea-surface temperature of 325 K. The red box in (a) isolates the rainfall event highlighted in panels (c and d), while the box in panel (b) isolates the rainfall event highlighted in panels (e and f). Red curves in panels (c–f) represent a propagation speed of 60 km hr^{-1}. These Hovmoller diagrams are averaged over the *Y* direction and are based on 2D instantaneous output.

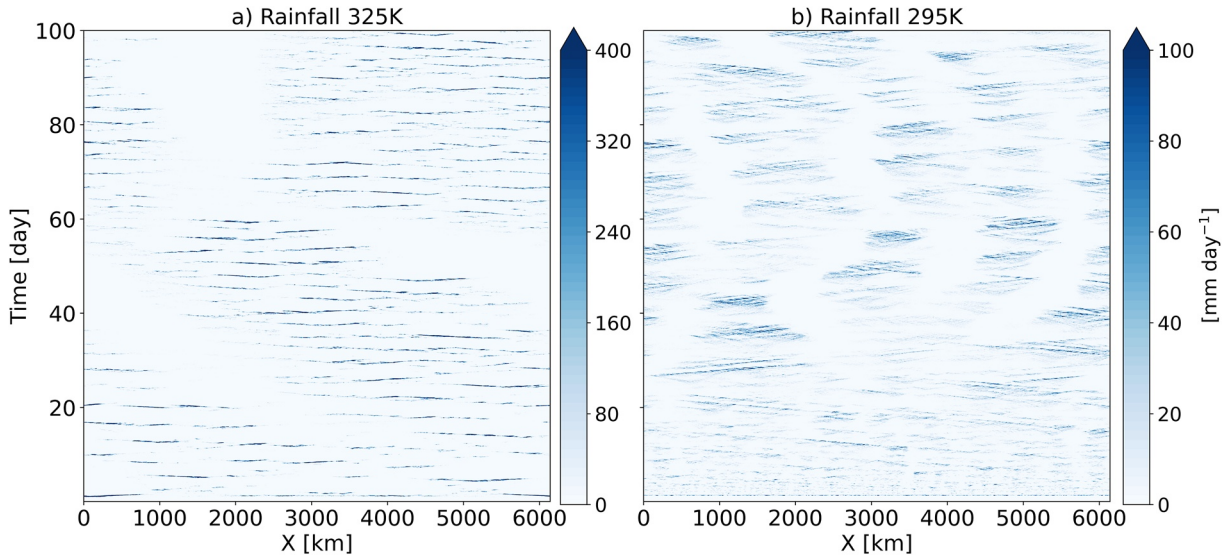

Figure 11. Hovmoller diagrams of the rainfall for radiative-convective-equilibrium large domain simulations under different sea surface temperatures: RCE_large_325 (a), and RCE_large_295 (b). These Hovmoller diagrams are averaged over the *Y* direction and are based on 2D instantaneous output.

day (as shown in Figure 10). With a propagation speed of 60 km hr^{-1} in each direction for 12 hr, a typical rainfall event covers a distance of roughly 1,500 km. Therefore, a typical event does not cover the entire domain, which has a length of over 6,000 km. We note that in the absence of rotation, gravity waves are the only possible explanation for this wavy behavior, as without Coriolis force, the characteristic features of Rossby and Kelvin waves would not emerge.

Figure 10 indicates that convective self-aggregation, along with the formation of the associated dry patches, modulates the oscillatory behavior of SW21 and its spatial scales. This can be observed by comparing the RCE_large simulation, which includes dry patches, and the RCE_large_FixedRAD simulation, which does not. In particular, we note that these oscillations do not occur in the dry patches when interactive radiation is present; the large-scale moist patches in the aggregated state provide an "envelope" within which the oscillatory convective regime is embedded. Moreover, a propagating precipitating event that reaches a transition between wet and dry patches quickly dissipates and stops propagating (Figures 10c and 10d). Hence, a characteristic localized outburst is generally smaller in RCE_large than in RCE_large FixedRAD simulations and the local return frequency of outbursts is greater.

Finally, we note from Figure 11 that also under the reference SST of 295 K gravity waves strongly modulate the local rainfall as was discussed before (Bretherton et al., 2006). However, under high SST the local rainfall occurs in much shorter and more intense events compared with the lower SST case (see also Figure S1 in Supporting Information S1) and with a peak in the power spectrum at shorter time scales (Figure 6). Since gravity waves affect the rainfall distribution under low SST without including the effect of the SW21 oscillatory behavior, we expect that the peak in the power spectrum of the local rainfall will correspond to the propagation time of gravity waves throughout the domain and hence will change linearly with domain size. To examine this expectation, we have conducted two additional simulations with different domain sizes under SST = 295 K (Table 1). It demonstrates that indeed under low SST the peak in the power spectrum of the local rainfall shifts to shorter periods as the domain becomes smaller and vanishes in the RCE_small (Figure S6 in Supporting Information S1), an effect that is not observed in high SST simulations for which the peak in the power spectrum is dominated by the SW21 oscillatory behavior and hence is at roughly constant period regardless of the domain size (including the RCE_small; Figure 6 and Figure S7 in Supporting Information S1). These results suggest that in large domain simulations there is a transition into a qualitative different precipitation regime under hothouse conditions compared with current climate conditions. This is similar to the results of SW21 that were based on small domain simulations.

To get a better feeling for the local precipitation at different places in the domain of the large domain hothouse simulation (RCE_large_325), in Figure 12 we divide the *x*-axis into 8 equal area parts (each span 768 km in the *x*-axis) and examine the rainfall time series and its power spectrum over the last 50 days of the simulations (area 1 corresponds to the first 768 km from the left in Figure 10a, and so on; the near surface MSE time evolution of these areas is presented in Figure S8 in Supporting Information S1). It demonstrates that areas which are in the

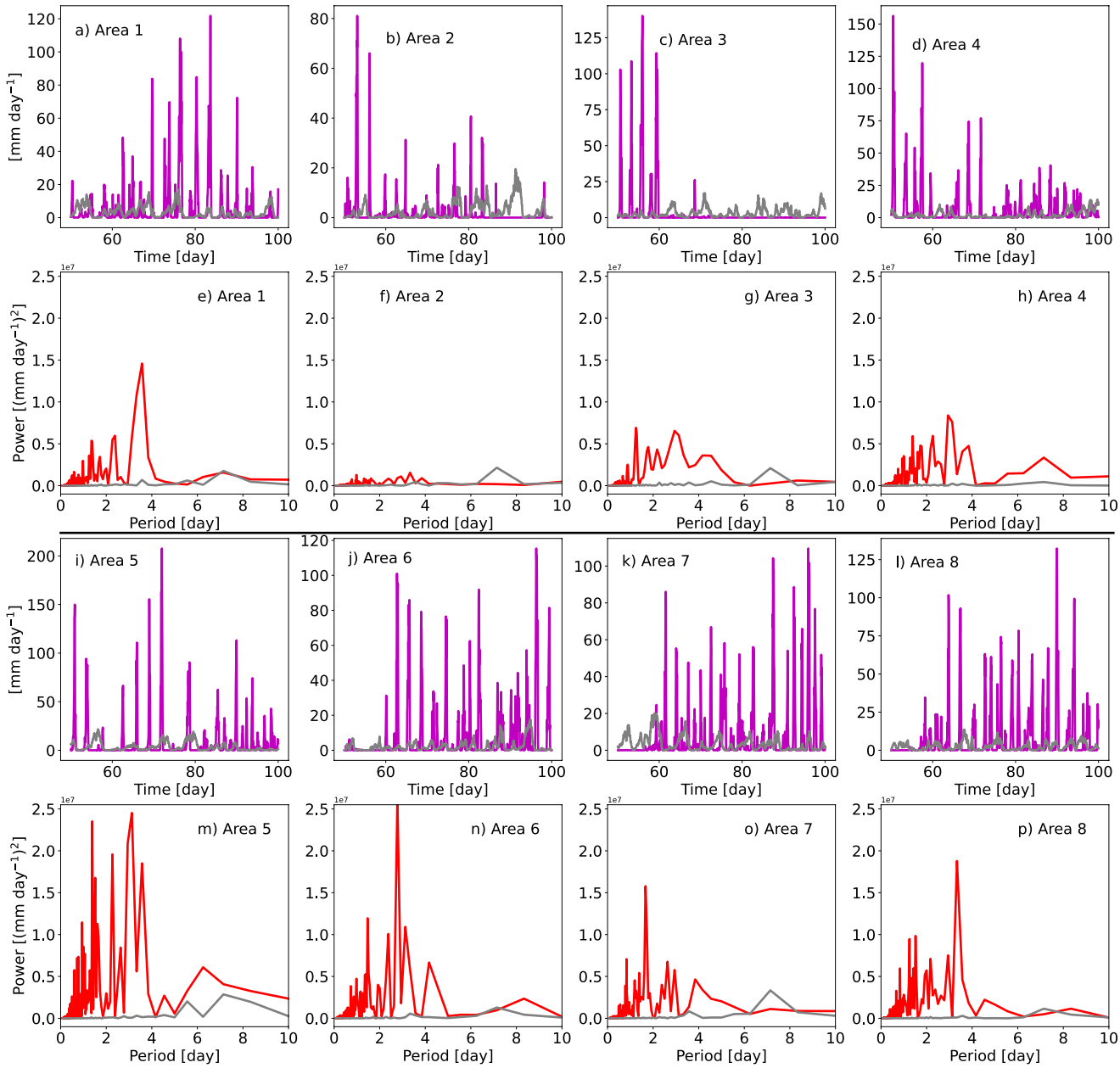

Figure 12. Rainfall time series and its power spectrum calculated for eight equal area parts (each span 768 km in the *x*-axis starting from the left of the domain) of the radiative-convective-equilibrium large domain simulations (RCE_large_325 and RCE_large_295 in gray for reference) over the last 50 days of the simulations.

rainy patches during the last 50 days of the simulations, and hence do not have long periods without rain, such as areas 1 and 8, demonstrate a strong peak in their power spectrum with a period of about 3 days, a peak which is not observed in the reference simulation. Areas in the domain which are found in the dry patch for a large portion of the last 50 days of the simulation, such as areas 2 and 3, demonstrate a less "well-defined" peak in the power spectrum. However, most areas demonstrate a local peak in the power spectrum at period somewhere between 2 and 4 days, which is partially averaged-out when examined over the entire domain, and hence results in a weak peak (Figure 6). The reference simulation (presented in gray in Figure 12) does not demonstrate this 3-day peak in any of the areas. However, it does show in some of the areas the weak peak discussed above at about 7-days period corresponding to the gravity-wave propagation time throughout the domain (Figure S6 in Supporting Information S1).

The conclusion from Figure 9, that the main difference between RCE_small and RCE_large is not due to the difference in convective aggregation and RHR vertical profile but rather related to the size of the domain and

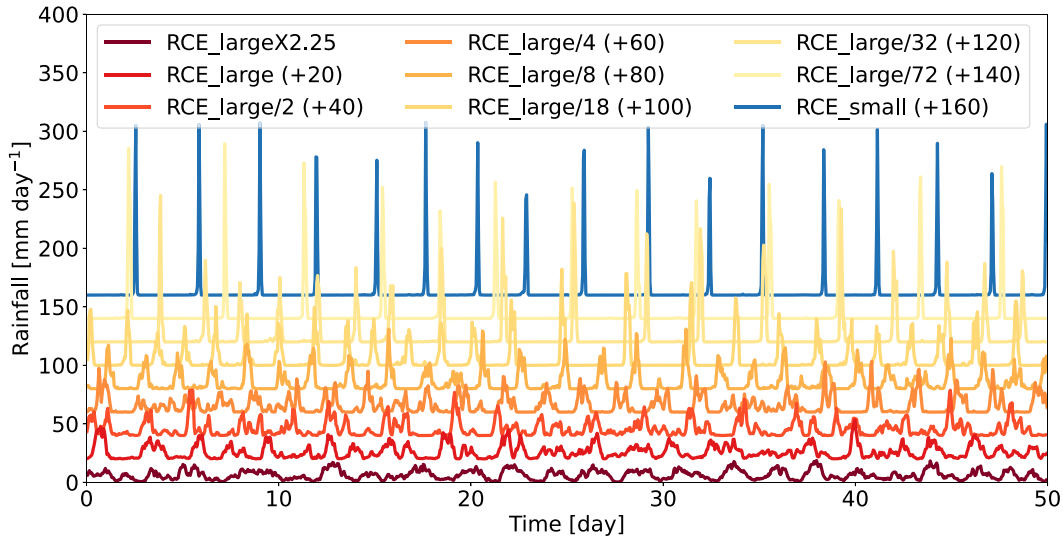

Figure 13. Domain-mean rainfall time series for simulations conducted with sea-surface temperature of 325 K and with different domain sizes. For clarity a specific offset value has been added to each curve, as noted in the legend.

the level of synchronization of the convection, invites examination of rainfall time series under a wide range of domain sizes (Table 1). Figure 13 illustrates that with the reduction in domain size the rainfall time series becomes more and more similar to the RCE_small simulation, trending toward distinct domain-mean rainfall outburst events separated by multiple dry days. That is to say that the rainfall becomes more synchronized throughout the domain as the domain size reduces. However, a power spectrum of the domain-mean rainfall (Figure S7 in Supporting Information S1) demonstrates that in all domain sizes examined here a peak is observed at somewhere between 2- and 3-days period. This peak is absent from the small and large domain low SST simulations, hence, strengthening the argument that there is a transition from a quasi-steady regime under low SST to an episodic deluge regime under high SST under all domain sizes.

The degree of rainfall synchronization throughout the domain can also be observed in the Hovmoller diagrams presented in Figure 14. It demonstrates that rainfall events that propagate across the domain cover an increasingly larger fraction of the domain as the domain size decreases. In RCE_small domain, where a propagation speed of 60 km hr^{-1} in each direction means that a rainfall event covers the entire domain in less than 1 hr (the output tempo-

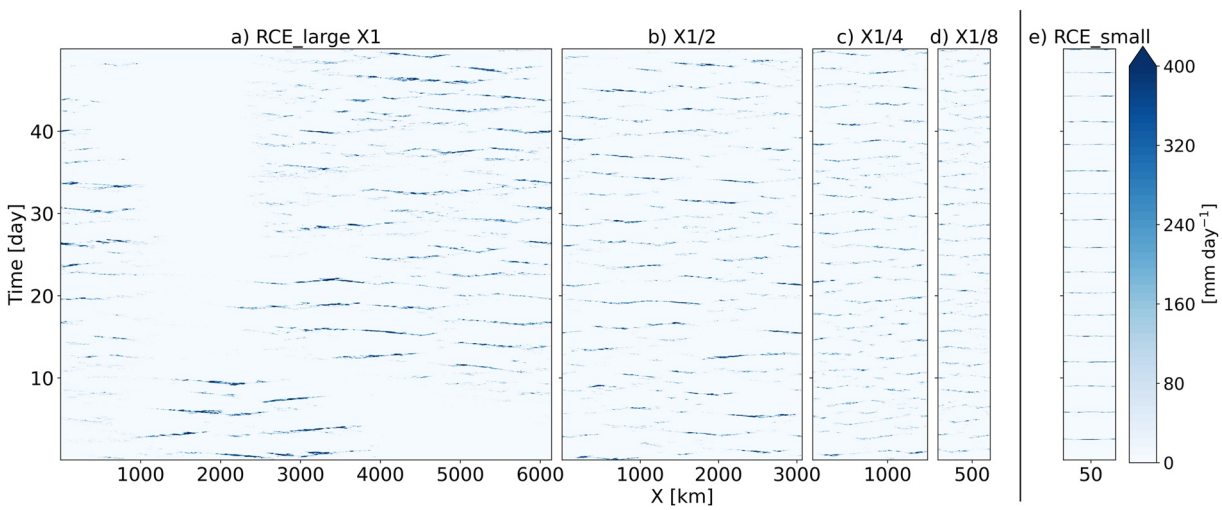

Figure 14. Hovmoller diagrams of the rainfall for simulations conducted with sea-surface temperature of 325 K and with different domain sizes, focused on the last 50 days of the simulations. Note that the radiative-convective-equilibrium small domain simulation (RCE_small) (e) is not to scale with the rest of the simulations. These Hovmoller diagrams are averaged over the *Y* direction and are based on 2D instantaneous output.

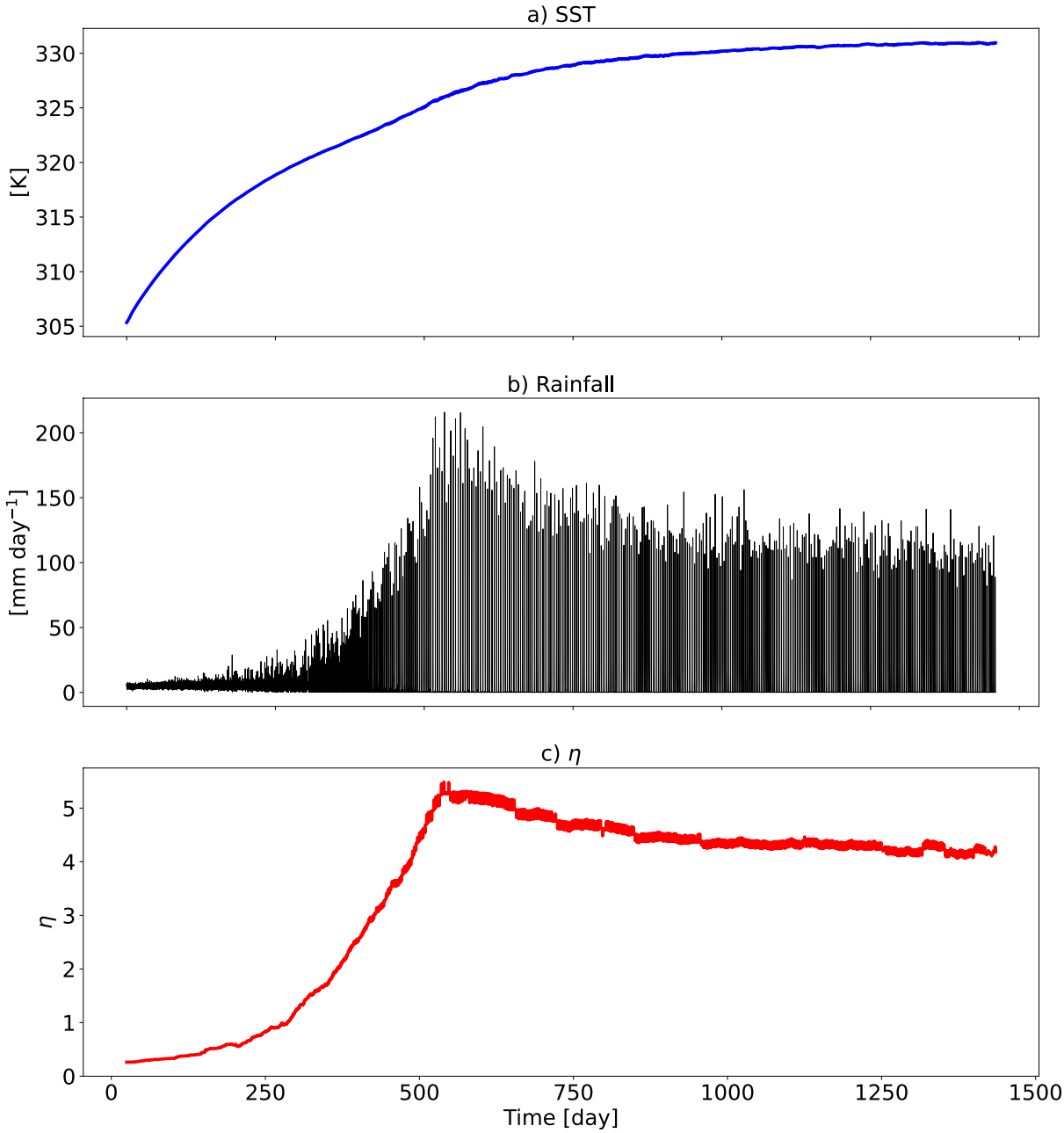

Figure 15. Radiative-convective-equilibrium simulation data from SW21: (a) the sea surface temperature (SST) and (b) the domain mean rainfall along with (c) the relative dispersion of the rainfall (η; defined as the ratio of the standard deviation to the mean) as a function of time. η is used here as a quantitative measure of the degree of synchronization of the rainfall throughout the domain and is calculated based on 50-day sliding window of the domain mean rainfall.

ral resolution), the precipitation events are shaped like delta functions, as seen in Figure 13. An examination of this simulation with 10-times higher output frequency demonstrates that in this case as well precipitation events propagate in the domain at the characteristic speed of gravity waves (Figures S9–S11 in Supporting Information S1).

To give a more quantitative measure of the degree of synchronization of the rainfall throughout the domain, in this paper we use the rainfall relative dispersion, η: the ratio of the standard deviation to the mean. High values of η represent a case in which the rainfall occurs mostly in short events with very high rates above the mean and long periods with no rain. Low values of η represent a steady regime of rainfall, with low standard deviations compared to the mean. The ability of η to capture the degree of rainfall synchronization throughout the domain is demonstrated in Figure 15, which presents the SST, domain-mean rainfall and η from the slab ocean RCE simu-

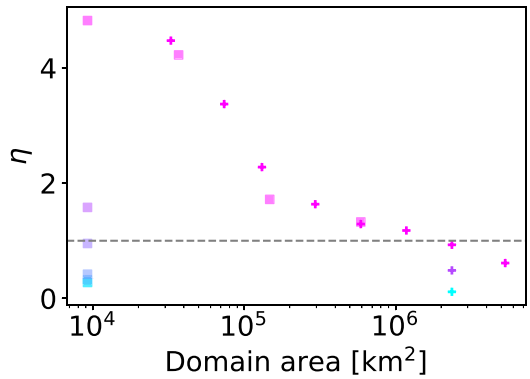

Figure 16. The relative dispersion of the rainfall (η; defined as the ratio of the standard deviation to the mean) for the different simulations conducted under homogeneous sea-surface temperature (SST) of 325 K and for the radiative-convective-equilibrium small domain (RCE_small) and large domain (RCE_large) simulations conducted under lower SSTs. These results are based on the last 50 days of each simulation. η is used here as a quantitative measure of the degree of synchronization of the rainfall throughout the domain. Square markers represent square domain simulations, plus markers represent rectangle domain simulations and the different colors represent different SSTs—colder coolers represent colder SST form 295–325 K in 5 K intervals. The dashed gray horizontal line mark $\eta = 1$ for reference.

lation of SW21. Specifically, it demonstrates that η sharply increases from values below 1, when the SST is closer to our current climate conditions (305 K), up to about 4–5 when the SST crosses the 325 K level.

Figure 16 presents η for all simulations conducted under homogeneous SST of 325 K and for the RCE_small and RCE_large simulations conducted with lower SSTs (Table 1). It demonstrates that indeed for both RCE_small and RCE_large η increases with SST as shown in Figure 15. In addition, Figure 16 demonstrates that η monotonically decreases with the domain size under SST of 325 K from roughly 5 to below 1; this is a similar range observed in the SW21 experiments shown in Figure 15. This trend suggests a lower degree of synchronization for larger domains. In addition, the geometry of the domain (rectangle vs. square domains) could potentially have an effect on the propagation of the convection throughout the domain and hence on the degree of synchronization. To examine that, Figure 16 presents three additional simulations (beside RCE_small) conducted with a square domain of different sizes (Table 1). It demonstrates that, at least for the cases examined here, the geometry of the domain does not affect the sensitivity of the degree of synchronization to domain size.

3.5. Effect of Convective Forced-Aggregation in Mock Walker Simulations

The simulations examined so far were conducted under homogeneous SST. Next we examine the three mock Walker hothouse simulations which were conducted under different domain sizes and resolutions (Table 1) and we compare it with a reference mock Walker simulation conducted under SST of 295 K. Comparing the large domain mock Walker simulations conducted under SST of 295 and 325 K (Figures 17a and 17b), we note that, as was reported before (Bretherton et al., 2006), even under the reference SST of 295 K gravity waves strongly modulate the precipitation. However, under high SST the local precipitation occurs in much shorter and more intense events compared with the lower

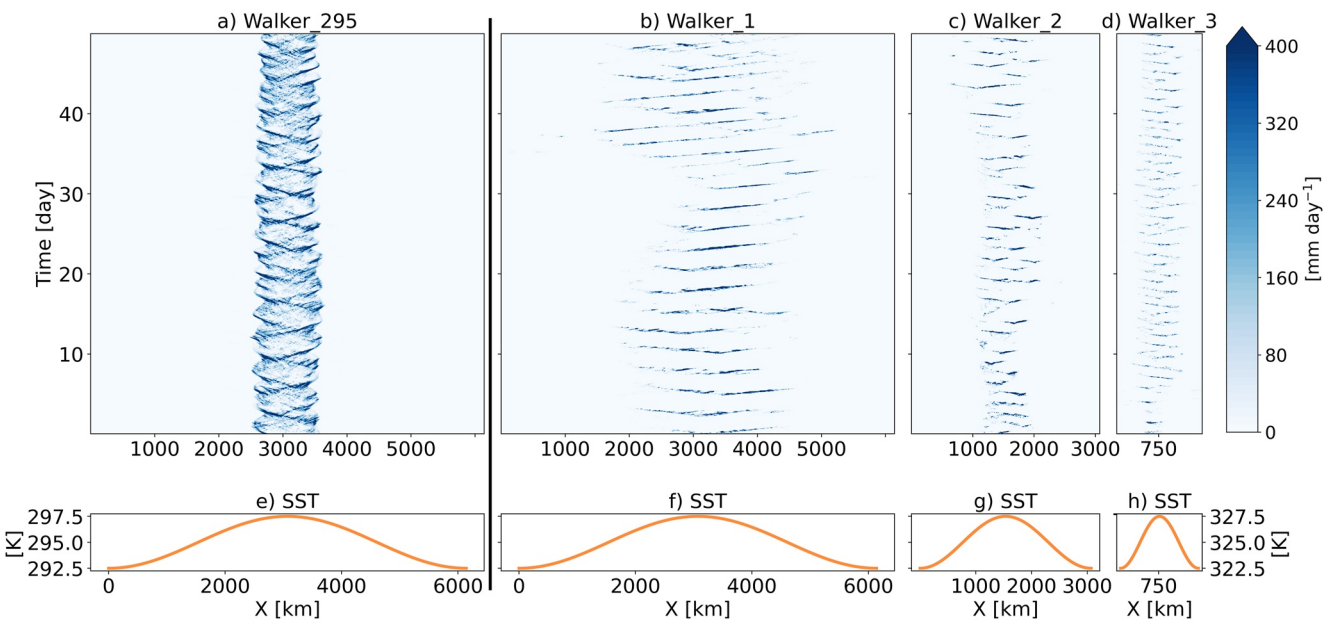

Figure 17. (a–d) Hovmoller diagrams of the rainfall for mock Walker simulations conducted with domain mean sea-surface temperature (SST) of 295 K (a) and 325 K (b–d) but with different domain sizes, focused on the last 50 days of the simulations. In panel (a) the rainfall is multiplied by 4. (e–h) The prescribed SST spatial distribution along the long dimension of the domain (X). These Hovmoller diagrams are averaged over the Y direction and are based on 2D instantaneous output.

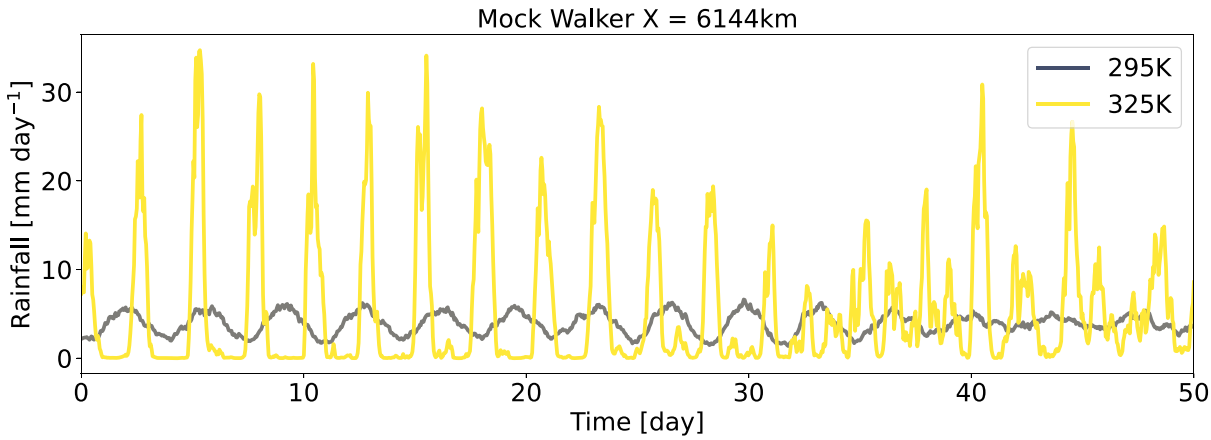

Figure 18. Domain-mean rainfall time series of the mock Walker simulations conducted with domain mean sea-surface temperature of 295 and 325 K.

SST case. On the domain-mean scale (Figure 18) the hothouse mock Walker simulation demonstrates a clear regularity with short periods with intense rainfall followed by periods without any rain in the entire domain. The reference mock Walker simulation on the other hand demonstrates much weaker oscillations (Bretherton et al., 2006). Figures 17b–17d demonstrates that, for all domain sizes examined here, even in the presence of SST-gradient forced large-scale circulation, short and intense outbursts of precipitation dominate the hydrological cycle of the hothouse climate. We note that these outbursts are concentrated around the center of the domain where the SST is warmest. In these simulations, which include large-scale circulation, there are persistent dry subsiding regimes present in the domain (at the two sides of the domain where the SST is lower than the domain mean). These persistent dry subsiding regimes act to enhance the longwave cooling of the atmosphere (Pierrehumbert, 1995; Figure S12 in Supporting Information S1), hence they act to weaken the domain-mean LTRH (Figure S13 in Supporting Information S1). Nevertheless, even this weak LTRH is enough to generate strong local rainfall oscillations (Figure 17; as was also noted in Section 3.2).

4. Conclusions

Hothouse climate conditions are believed to have existed in the history of our planet (Charnay et al., 2017; Meckler et al., 2022; Sleep, 2010) and they will very likely form in its distant future (Seeley & Wordsworth, 2021; Wolf & Toon, 2015). Little is known concerning convection under these hot conditions, let alone about convective-aggregation.

In this paper, we have examined the claims of Seeley and Wordsworth (2021, SW21), which showed that under hothouse conditions convection shifts into a "relaxation oscillator" regime characterized by short and intense outbursts of rainfall separated by multi-day dry spells. The driver for this shift is the lower-tropospheric radiative heating (LTRH) that characterizes hothouse conditions. Using a series of simulations, we have demonstrated that the LTRH is sufficient but not necessary for the formation of the relaxation oscillator regime. Under relatively low SST, which is common in our current climate condition, the relaxation oscillator regime is formed when LTRH is present (as was also shown in SW21). On the other hand, under high SST hothouse conditions the LTRH does not have to be positive (but it does have to be relatively high) for the formation of the relaxation oscillator regime. The fact that the relaxation oscillator regime could form under current climate conditions has implications for radiative changes by shortwave absorbing substances such as absorbing aerosols.

SW21's conclusions were based on small domain simulations which prohibit "traditional" spatial convective self-aggregation (Muller & Held, 2012). Hence, it was unclear from SW21 what happens to this oscillatory behavior when traditional self-aggregation is allowed in a larger domain or what the spatial scale is of the oscillations in SW21. To answer these questions we conducted a series of RCE simulations with different domain sizes and geometries under hothouse conditions (Table 1).

Comparing small and large domains, convection-permitting hothouse climate simulations demonstrate that SW21's oscillatory behavior, which appears in small domain simulations, becomes much less coherent in the spatial mean of large domain simulations. In addition, these simulations demonstrate that "traditional" convec-

tive self-aggregation (Muller et al., 2022) is formed under hothouse conditions when the domain is large enough to allow it (Muller & Held, 2012). Similar to our current climate conditions, convective self-aggregation in hothouse climates dries the atmosphere, enhancing the OLR and weakening the LTRH. However, large-domain simulations with prescribed RHRs demonstrate that preventing convective self-aggregation and its dampening effect on the LTRH does not bring the large-domain simulations back to the strong oscillatory behavior seen in the small domain simulations. Hence, we conclude that while convective self-aggregation modulates the spatial distribution of convection in hothouse climates, it cannot explain the difference seen between small and large domain simulations. Instead, we demonstrate that the degree of synchronization of the convection throughout the domain decreases with the domain size. More specifically, we suggest that gravity waves are responsible for the synchronization of the convection. The propagation speed of the gravity waves (which is a few 10s km h^{-1}) and the domain size, determine the degree of synchronization, which can be measured by the domain mean rainfall relative dispersion (ratio of standard deviation to mean).

In addition, we examine the effect of an idealized SST-forced large-scale circulation on SW21's oscillatory behavior in mock Walker simulations with different domain sizes. The imposed large-scale circulation forces the convection to aggregate along the regions of higher SST. However, we have demonstrated that the convection still occurs in short and intense outbursts, not seen under current climate conditions, even in the presence of large-scale circulation. These outburst events occur despite the fact that the presence of large-scale circulation acts to weaken the LTRH by enhancing the OLR at the subsiding regions.

As noted in SW21, the oscillatory behavior has analogs in our current climate conditions. Specifically, temporal oscillations in convection have been reported for deep convective clouds (Yano & Plant, 2012), shallow convective clouds (Dagan et al., 2018) and even marine strato-cumulus clouds (Feingold et al., 2010). In the former two cases (deep and shallow convection), cycles of recharge-discharge of thermodynamic instability were identified (Bladé & Hartmann, 1993; Dagan et al., 2018; Yano & Plant, 2012). The mechanism behind these oscillations is as follows: once sufficient convective available potential energy accumulates in the atmosphere, convection initiates and acts to consume the instability until the convection stops. Next the instability builds up again by surface fluxes and radiative cooling until it launches another cycle (Dagan et al., 2018; Yano & Plant, 2012). The addition of the LTRH under hothouse conditions could strongly intensify these oscillations and make them dominate the local precipitation distribution. In addition, under hothouse conditions an additional mechanism, as proposed by SW21 is in play involving the formation of virga and associated evaporative cooling that triggers an outburst. Hence, based on the results presented here, we speculate that under extreme global warming scenarios, an oscillatory behavior will become more pronounced in the warmest parts of the globe, which could have strong implications for extreme precipitation (Knapp et al., 2008; Pendergrass, 2018).

Data Availability Statement

The model SAM is publicly available in M. Khairoutdinov (2023). The data presented in this study is publicly available in Dagan et al. (2023). The code used for calculating I_{org} is publicly available in Wing (2023).

Acknowledgments
This research has been supported by the Israel Science Foundation (Grant 1419/21). The authors thank Yonatan Goldsmith for very fruitful discussions during the preparation of this paper.

References

Bao, J., Sherwood, S. C., Colin, M., & Dixit, V. (2017). The robust relationship between extreme precipitation and convective organization in idealized numerical modeling simulations. *Journal of Advances in Modeling Earth Systems*, *9*(6), 2291–2303. https://doi.org/10.1002/2017ms001125

Bladé, I., & Hartmann, D. L. (1993). Tropical intraseasonal oscillations in a simple nonlinear model. *Journal of the Atmospheric Sciences*, *50*(17), 2922–2939. https://doi.org/10.1175/1520-0469(1993)050<2922:tioias>2.0.co;2

Bony, S., Stevens, B., Frierson, D. M., Jakob, C., Kageyama, M., Pincus, R., et al. (2015). Clouds, circulation and climate sensitivity. *Nature Geoscience*, *8*(4), 261–268. https://doi.org/10.1038/ngeo2398

Bretherton, C. S., Blossey, P. N., & Khairoutdinov, M. (2005). An energy-balance analysis of deep convective self-aggregation above uniform SST. *Journal of the Atmospheric Sciences*, *62*(12), 4273–4292. https://doi.org/10.1175/jas3614.1

Bretherton, C. S., Blossey, P. N., & Peters, M. E. (2006). Interpretation of simple and cloud-resolving simulations of moist convection–radiation interaction with a mock-walker circulation. *Theoretical and Computational Fluid Dynamics*, *20*(5), 421–442. https://doi.org/10.1007/s00162-006-0029-7

Charnay, B., Le Hir, G., Fluteau, F., Forget, F., & Catling, D. C. (2017). A warm or a cold early Earth? New insights from a 3-D climate-carbon model. *Earth and Planetary Science Letters*, *474*, 97–109. https://doi.org/10.1016/j.epsl.2017.06.029

Collins, W. D., Rasch, P. J., Boville, B. A., Hack, J. J., McCaa, J. R., Williamson, D. L., et al. (2006). The formulation and atmospheric simulation of the Community Atmosphere Model version 3 (CAM3). *Journal of Climate*, *19*(11), 2144–2161. https://doi.org/10.1175/jcli3760.1

Coppin, D., & Bony, S. (2015). Physical mechanisms controlling the initiation of convective self-aggregation in a general circulation model. *Journal of Advances in Modeling Earth Systems*, *7*(4), 2060–2078. https://doi.org/10.1002/2015ms000571

Dagan, G., Koren, I., Kostinski, A., & Altaratz, O. (2018). Organization and oscillations in simulated shallow convective clouds. *Journal of Advances in Modeling Earth Systems*, *10*(9), 2287–2299. https://doi.org/10.1029/2018ms001416

Dagan, G., Seeley, J. T., & Steiger, N. (2023). Data for the paper: Convection and convective-organization in hothouse climates [Dataset]. Zenodo. https://doi.org/10.5281/zenodo.8054055

Da Silva, N. A., Muller, C., Shamekh, S., & Fildier, B. (2021). Significant amplification of instantaneous extreme precipitation with convective self-aggregation. *Journal of Advances in Modeling Earth Systems*, *13*(11), e2021MS002607. https://doi.org/10.1029/2021ms002607

Dingley, B., Dagan, G., & Stier, P. (2021). Forcing convection to aggregate using diabatic heating perturbations. *Journal of Advances in Modeling Earth Systems*, *13*(10), e2021MS002579. https://doi.org/10.1029/2021ms002579

Feingold, G., Koren, I., Wang, H., Xue, H., & Brewer, W. A. (2010). Precipitation-generated oscillations in open cellular cloud fields. *Nature*, *466*(7308), 849–852. https://doi.org/10.1038/nature09314

Fildier, B., Collins, W. D., & Muller, C. (2021). Distortions of the rain distribution with warming, with and without self-aggregation. *Journal of Advances in Modeling Earth Systems*, *13*(2), e2020MS002256. https://doi.org/10.1029/2020ms002256

Grabowski, W. W., Yano, J.-I., & Moncrieff, M. W. (2000). Cloud resolving modeling of tropical circulations driven by large-scale SST gradients. *Journal of the Atmospheric Sciences*, *57*(13), 2022–2040. https://doi.org/10.1175/1520-0469(2000)057<2022:crmotc>2.0.co;2

Hartmann, D. L., & Larson, K. (2002). An important constraint on tropical cloud-climate feedback. *Geophysical Research Letters*, *29*(20), 12–21. https://doi.org/10.1029/2002gl015835

Hohenegger, C., & Jakob, C. (2020). A relationship between ITCZ organization and subtropical humidity. *Geophysical Research Letters*, *47*(16), e2020GL088515. https://doi.org/10.1029/2020gl088515

Jeevanjee, N., & Romps, D. M. (2018). Mean precipitation change from a deepening troposphere. *Proceedings of the National Academy of Sciences*, *115*(45), 11465–11470. https://doi.org/10.1073/pnas.1720683115

Khairoutdinov, M. (2023). SAM model code [Software]. Retrieved from http://rossby.msrc.sunysb.edu/~marat/SAM.html

Khairoutdinov, M. F., & Randall, D. A. (2003). Cloud resolving modeling of the arm summer 1997 IOP: Model formulation, results, uncertainties, and sensitivities. *Journal of the Atmospheric Sciences*, *60*(4), 607–625. https://doi.org/10.1175/1520-0469(2003)060<0607:crmota>2.0.co;2

Knapp, A. K., Beier, C., Briske, D. D., Classen, A. T., Luo, Y., Reichstein, M., et al. (2008). Consequences of more extreme precipitation regimes for terrestrial ecosystems. *BioScience*, *58*(9), 811–821. https://doi.org/10.1641/b580908

kumar Kopparapu, R., Wolf, E. T., Haqq-Misra, J., Yang, J., Kasting, J. F., Meadows, V., et al. (2016). The inner edge of the habitable zone for synchronously rotating planets around low-mass stars using general circulation models. *The Astrophysical Journal*, *819*(1), 84. https://doi.org/10.3847/0004-637x/819/1/84

Lutsko, N., & Cronin, T. W. (2023). Mock-Walker simulations: Mean climates, responses to warming and transition to double-cell circulations. *Authorea Preprints*. https://doi.org/10.22541/essoar.167591087.76248356/v1

Meckler, A. N., Sexton, P., Piasecki, A., Leutert, T., Marquardt, J., Ziegler, M., et al. (2022). Cenozoic evolution of deep ocean temperature from clumped isotope thermometry. *Science*, *377*(6601), 86–90. https://doi.org/10.1126/science.abk0604

Muller, C., & Held, I. M. (2012). Detailed investigation of the self-aggregation of convection in cloud-resolving simulations. *Journal of the Atmospheric Sciences*, *69*(8), 2551–2565. https://doi.org/10.1175/jas-d-11-0257.1

Muller, C., Yang, D., Craig, G., Cronin, T., Fildier, B., Haerter, J. O., et al. (2022). Spontaneous aggregation of convective storms. *Annual Review of Fluid Mechanics*, *54*(1), 133–157. https://doi.org/10.1146/annurev-fluid-022421-011319

Müller, S. K., & Hohenegger, C. (2020). Self-aggregation of convection in spatially varying sea surface temperatures. *Journal of Advances in Modeling Earth Systems*, *12*(1), e2019MS001698. https://doi.org/10.1029/2019ms001698

Pendergrass, A. G. (2018). What precipitation is extreme? *Science*, *360*(6393), 1072–1073. https://doi.org/10.1126/science.aat1871

Pendergrass, A. G. (2020). Changing degree of convective organization as a mechanism for dynamic changes in extreme precipitation. *Current Climate Change Reports*, *6*(2), 47–54. https://doi.org/10.1007/s40641-020-00157-9

Pendergrass, A. G., Reed, K. A., & Medeiros, B. (2016). The link between extreme precipitation and convective organization in a warming climate: Global radiative-convective equilibrium simulations. *Geophysical Research Letters*, *43*(21), 11–445. https://doi.org/10.1002/2016gl071285

Pierrehumbert, R. T. (1995). Thermostats, radiator fins, and the local runaway greenhouse. *Journal of the Atmospheric Sciences*, *52*(10), 1784–1806. https://doi.org/10.1175/1520-0469(1995)052<1784:trfatl>2.0.co;2

Popp, M., Schmidt, H., & Marotzke, J. (2016). Transition to a moist greenhouse with CO_2 and solar forcing. *Nature Communications*, *7*(1), 10627. https://doi.org/10.1038/ncomms10627

Seeley, J. T., & Wordsworth, R. D. (2021). Episodic deluges in simulated hothouse climates. *Nature*, *599*(7883), 74–79. https://doi.org/10.1038/s41586-021-03919-z

Sleep, N. H. (2010). The Hadean-Archaean environment. *Cold Spring Harbor Perspectives in Biology*, *2*(6), a002527. https://doi.org/10.1101/cshperspect.a002527

Sobel, A. H., Nilsson, J., & Polvani, L. M. (2001). The weak temperature gradient approximation and balanced tropical moisture waves. *Journal of the Atmospheric Sciences*, *58*(23), 3650–3665. https://doi.org/10.1175/1520-0469(2001)058<3650:twtgaa>2.0.co;2

Song, X., Abbot, D. S., & Yang, J. (2023). Critical role of vertical radiative cooling contrast in triggering episodic deluges in small-domain hothouse climates. *arXiv preprint arXiv:2307.01219*.

Spaulding-Astudillo, F. E., & Mitchell, J. L. (2023). The emergence of relaxation-oscillator convection on Earth and Titan. *arXiv preprint arXiv:2306.03219*.

Tompkins, A. M., & Semie, A. G. (2017). Organization of tropical convection in low vertical wind shears: Role of updraft entrainment. *Journal of Advances in Modeling Earth Systems*, *9*(2), 1046–1068. https://doi.org/10.1002/2016ms000802

Wing, A. A. (2023). The code used for calculating i_{org} [Software]. Retrieved from https://myweb.fsu.edu/awing/rcemipsims.html

Wing, A. A., Emanuel, K., Holloway, C. E., & Muller, C. (2018). Convective self-aggregation in numerical simulations: A review. *Shallow Clouds, Water Vapor, Circulation, and Climate Sensitivity*, *65*, 1–25.

Wing, A. A., & Emanuel, K. A. (2014). Physical mechanisms controlling self-aggregation of convection in idealized numerical modeling simulations. *Journal of Advances in Modeling Earth Systems*, *6*(1), 59–74. https://doi.org/10.1002/2013ms000269

Wing, A. A., Reed, K. A., Satoh, M., Stevens, B., Bony, S., & Ohno, T. (2018). Radiative–convective equilibrium model intercomparison project. *Geoscientific Model Development*, *11*(2), 793–813. https://doi.org/10.5194/gmd-11-793-2018

Wing, A. A., Stauffer, C. L., Becker, T., Reed, K. A., Ahn, M.-S., Arnold, N. P., et al. (2020). Clouds and convective self-aggregation in a multi-model ensemble of radiative-convective equilibrium simulations. *Journal of Advances in Modeling Earth Systems*, *12*(9), e2020MS002138. https://doi.org/10.1029/2020ms002138

Wolf, E., Haqq-Misra, J., & Toon, O. (2018). Evaluating climate sensitivity to CO_2 across Earth's history. *Journal of Geophysical Research: Atmospheres*, *123*(21), 11–861. https://doi.org/10.1029/2018jd029262

Wolf, E., & Toon, O. (2015). The evolution of habitable climates under the brightening Sun. *Journal of Geophysical Research: Atmospheres*, *120*(12), 5775–5794. https://doi.org/10.1002/2015jd023302

Yang, D. (2018). Boundary layer diabatic processes, the virtual effect, and convective self-aggregation. *Journal of Advances in Modeling Earth Systems*, *10*(9), 2163–2176. https://doi.org/10.1029/2017ms001261

Yano, J.-I., & Plant, R. (2012). Finite departure from convective quasi-equilibrium: Periodic cycle and discharge–recharge mechanism. *Quarterly Journal of the Royal Meteorological Society*, *138*(664), 626–637. https://doi.org/10.1002/qj.957